Annu. Rev. Phys. Chem. 1992. 43:627–61

EQUILIBRIUM AND DYNAMIC PROCESSES AT INTERFACES BY SECOND HARMONIC AND SUM FREQUENCY GENERATION

Kenneth B. Eisenthal

Department of Chemistry, Columbia University, New York, NY 10027

KEY WORDS: interface chemical reactions, interface dynamics, interface orientational structure, monolayers and surfactants

INTRODUCTION

Interfaces are ubiquitous. They occur everywhere. They are the boundaries that separate distinct physical and chemical regions of matter. The bulk materials on adjacent sides of the interface can be chemically identical, as with a liquid water/vapor water interface, or they can be chemically different, as at a liquid/liquid interface such as hexadecane/water. All transfers of chemical species between the bulk regions must cross the interface. But, aside from mediating all exchanges, the interface has unique chemical and physical properties, which differ from either bulk medium. Because of these properties, the interface has fundamental scientific and technological importance (1).

The origin of the distinctive interface properties is the asymmetry in forces that molecules and atomic species experience there, together with the almost two-dimensional geometry of the interface. These features are manifested in such things as the chemical composition at an interface. For example, even when the water concentration greatly exceeds that of alcohol in a bulk alcohol-water solution, we would find that the composition is almost exclusively alcohol at the vapor/solution interface. As with alcohol-water, the chemical compositions of the interface and the surrounding

0066–426X/92/1101–0627$02.00

bulk media are usually different. Because of the asymmetry of forces at an interface, the structural, i.e. the geometrical, arrangement of molecules at an interface differs from that in the bulk media. Consider the vapor/alcohol-water solution interface. Due to hydrophobic and hydrophilic forces, the hydrocarbon part of the alcohol extends into the vapor, whereas the polar hydroxy moiety points to the bulk solution. On the other hand, in the solution and vapor, the alcohol and water molecules are isotropically oriented, because the time-averaged forces are isotropic. As a result of the unique chemical composition and structure of the interface, its dielectric properties (e.g. polarity) and transport properties (e.g. viscosity) differ from those of the adjacent bulk media. Considering these various factors, equilibrium and dynamic properties are markedly different in the interfacial and bulk regions.

Despite the widespread interest in interfaces, ranging from the pure sciences to medicine and engineering, it remains difficult to probe interfaces, especially buried ones, e.g. liquid/liquid and liquid/solid interfaces. It is hard to apply the powerful methods of spectroscopy on interfacial problems: If the interfacial molecules of interest are also present in either bulk medium, then any spectroscopic signal will probably be dominated by the overwhelmingly larger population in the bulk. Fortunately, sufficient energy shifts in the spectra of interfacial molecules sometimes occur, thereby making it possible to differentiate them from bulk molecules. Even then, however, the spectral widths can be problematic and certainly limiting. When the molecules of interest are only present in the interface, e.g. long-chain lipids at an air/water interface, this problem of separating interface from bulk absorption or emission is not present. Generally, however, the molecules of interest are present in the bulk solution, as well as in the interface. In fact, an important issue is the energetics and dynamics that drive or repel molecules and ions to and from the bulk and interface.

In recent years, the important and promising nonlinear method of second harmonic generation (SHG) has been advanced. The new spectroscopic method has now extended to and includes the related method of sum frequency generation (SFG) (2–5). In SHG, light at a frequency ω interacts with a nonlinear medium to generate radiation at 2ω; in SFG, light at two different frequencies, ω_1, and ω_2, generate radiation at the sum frequency, $\omega_1+\omega_2$. These nonlinear techniques are proving to be extremely powerful in studying equilibrium and dynamic processes at interfaces. The key feature of SHG and SFG is that they are electric-dipole forbidden in centrosymmetric media (2–5). Therefore, liquids and gases, which are clearly centrosymmetric, as well as centrosymmetric solids, do not generate strong signals from the bulk. At the interface, however, the

inversion symmetry is broken, and SHG becomes electric-dipole allowed, thereby mitigating the problem of large signals from the adjacent bulk media.

ORIENTATIONAL STRUCTURE: MOLECULAR ORIENTATION AT INTERFACES

The intermolecular interactions of adsorbates with surrounding molecules determine the orientation of interfacial molecules. Knowledge of the orientational structure at interfaces and, thus, the intermolecular forces can be obtained from measurements of the polarization of the SH light (6–10). The relation between the measured macroscopic nonlinear susceptibility elements $\chi^{(2)}$, which are in the laboratory axis frame, and the nonlinear polarizability elements $\alpha^{(2)}$, which are in the molecular axis frame, yield orientational information on the molecules at the interface.

Orientation at the Air/Water Interface

One example of such measurements at the air/water interface showed a very strong dependence of the orientations of insoluble amphiphiles on the presence of organic solutes in the bulk and interfacial regions (11). Although the head groups of the amphiphiles were similar, the addition of hydroxybenzoic acid (HO–C_6H_4–COOH) to the water solution affected their orientations very differently.

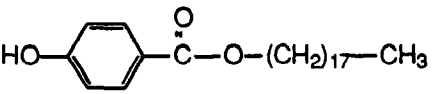

1.

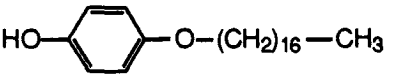

2.

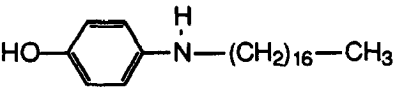

3.

For Case 1, there was no effect; for Cases 2 and 3, no SH signal was detected in the presence of the solute. The absence of a SH signal was attributed to a flat orientation, i.e. an orientation that would give no SH signal for the unperturbed molecule. Although other unknown factors could be responsible for these observations, the effect is nonetheless dra-

matic. A further demonstration of the specificity of the interface solute-amphiphile interaction was the following observation for the second amphiphile: The addition of a single methylene group to the hydroxybenzoic acid (HO–C_6H_4–CH_2–COOH) yielded an observable signal; for the unsubstituted hydroxybenzoic acid, no SH signal was observed, presumably because the hydroxybenzoic acid induced the head groups to assume a flat orientation.

A further example, which demonstrates the sensitivity of a single additional methylene group to a long-chain amphiphile, is the effect on the orientation at the air/water interface of nitroaniline terminated monolayers of

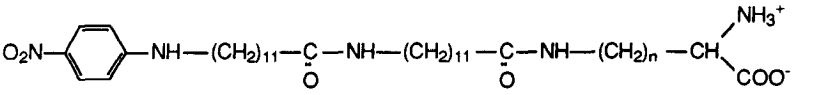

where n was 3 or 4 (12). The tilt angle of the nitroaniline head groups, assuming a narrow distribution of orientations, was 55° for the $n = 3$ compound and 75° for the $n = 4$ compound. This large effect on the orientational ordering of a terminal group was attributed to the alignment of the amino acid head groups of adjacent molecules, together with intermolecular hydrogen bonding between the amide groups of adjacent chains. If the chains are rigid, then the addition of a single methylene can greatly alter the tilt angles of the terminal nitroaniline groups.

Shirota et al (13) have conducted experiments on monolayers at the air/water interface of a binary mixture of the long-chain amphiphiles, hemicyanine dye $C_{22}H_{45}$–N^+–C_5H_4–$(CH)_2$–C_6H_4–N–$(CH_3)_2$, and arachidic acid $CH_3(CH_2)_{18}COOH$. They found that the tilt angle of the hemicyanine head groups decreased (moved towards the surface normal) as the fraction of the hemicyanine containing amphiphile increased.

In a noteworthy series of experiments, Vogel et al (14) questioned whether the subsurface layer of molecules, located beneath an orientationally ordered surface layer at the air/water interface, is orientationally ordered. They found that a soluble naphthalensulfonate amphiphile, CH_3–$(CH_2)_5$–$C_{10}H_6$–SO_3Na, did not form an orientationally ordered layer beneath an insoluble close packed monolayer of CH_3–$(CH_2)_{17}$–$C_{10}H_6$–SO_3Na.

Monolayer Penetration by Bulk Solute Molecules

Researchers have long been interested in the effect of an insoluble monolayer on the adsorption of surface-active solutes from the bulk, often

referred to as monolayer penetration (1). Aside from fundamental chemistry and physics, monolayer penetration is relevant to other areas, such as biological interfaces, in which the penetration of a biological membrane (bilayer) by solute molecules is important to biological function (15). Zhao et al (16) used SHG to study the orientation and population of p-nitrophenol (PNP) at an air/water interface containing fatty acids. They found that the interface PNP population increased by up to a factor of two when a fatty acid, pentadecanoic acid $CH_3(CH_2)_{13}COOH$, or hexadecanoic acid $CH_3(CH_2)_{14}COOH$ was spread onto the air/water interface. However, as the fatty acid density was increased beyond 50 $Å^2$ per fatty acid molecule, the PNP population decreased, thus finally achieving a population at 20 $Å^2$, which is well below that of PNP with no fatty acid present. Beyond a certain packing, the PNP cannot remain in the surface and is squeezed out. Second harmonic measurements demonstrated that the orientation of the PNP molecules also changed as the fatty acid density increased. The PNP molecules shifted their orientation toward the surface normal, thereby occupying a smaller surface area as the fatty acid packing became tighter. Interestingly, the behavior of PNP for both the C_{15} and C_{16} fatty acids is the same, despite the fact that the C_{15} and C_{16} surface phase diagrams are very different. The different phase diagrams are mainly due to the different interactions between the hydrophobic chains of the respective acids. The SH results suggest that the PNP molecules are not located in the chain region of the interface, but rather near the polar head group of the fatty acids, which are the same for the C_{15} and C_{16} acids.

Orientation at Air/Solid Interfaces

In discussing the average angle of orientation of a symmetry axis of a molecule with respect to the surface normal, it is often assumed that one of the nonlinear polarizability elements $\alpha^{(2)}$ dominates. This may or may not be the case, depending on the molecule and on the wavelength of the light used. By combining SH measurements of the nonlinear susceptibility elements (8, 10, 17) at several wavelengths with theoretical calculations to determine the important $\alpha^{(2)}$ elements, the orientation of the long axis of methylene blue (17),

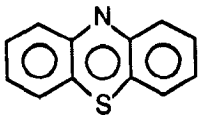

adsorbed on a silica surface was 58° with respect to the surface normal.

Higgins et al (17) found that contributions from more than one element of $\alpha^{(2)}$ contributed to the SH signal.

Peterson & Harris (18) have shown that by combining polarized SHG measurements with measured shifts in the absorption spectrum, information on the orientation of the monomers with respect to each other, i.e. dimer geometry, as well as with the surface normal, can be obtained. These ideas were applied to a rhodamine B monolayer adsorbed on a quartz substrate. By combining SH polarization measurements (6) and spectral shift measurements (18, 19), a parallel orientation of the long axes of the monomers in the dimer geometry was obtained, with their long axes oriented at 52° with the surface normal. The combination of resonant SHG measurements at two absorptions that have perpendicular transition dipoles with spectral shift measurements can be particularly valuable in studying molecular aggregates at surfaces. Of course, to measure the spectral shifts, one cannot usually use adsorbates that are also present in the adjacent bulk media.

ABSOLUTE MOLECULAR ORIENTATION: POLAR ORDERING AT INTERFACES

The orientational structural studies discussed above have provided information on the angle of a specified molecular axis with respect to the surface normal. From the data collected in these studies, the absolute orientation (polar alignment) of the molecules, i.e. which end of the molecule points up versus down, cannot be obtained, because the polarization of the SH light depends on the ratio of the $\chi^{(2)}$ elements. If the molecules were pointing up or down, the ratio of the $\chi^{(2)}$ elements and, thus, the polarization of the SH light would be the same. This can be seen by carrying out a reflection in the surface plane, an operation that reverses the direction of the molecules. Because all of the $\chi^{(2)}$ elements change sign on this reflection, the ratio of $\chi^{(2)}$ elements and, hence, the polarization of the SH light remain unchanged. Although the ratio of $\chi^{(2)}$ elements cannot yield the absolute molecular orientation, Kemnitz et al (20) recognized that the sign of any $\chi^{(2)}$ element, commonly referred to as the phase of $\chi^{(2)}$, contains information on the absolute orientation of the adsorbate. A simple demonstration of this occurs when a single element $\alpha^{(2)}_{zzz}$ along the molecular z axis dominates. The independent elements are,

$$\chi^{(2)}_{zzz} = N_S \langle \cos^3 \theta \rangle \alpha^{(2)}_{zzz}$$

$$\chi^{(2)}_{xzx} = \tfrac{1}{2} N_S \langle \cos \theta \sin^2 \theta \rangle \alpha^{(2)}_{zzz},$$

where N_S is the adsorbate density, and θ is the angle that the molecular

axis z makes with the surface normal Z. The laboratory X axis lies in the surface plane, and the elements containing Y are the same as those containing X. We see from these equations that if the sign of a $\chi^{(2)}$ element is positive, then the product of the angular factor and the $\alpha^{(2)}$ must also be positive. Then, if $\alpha^{(2)}$ is known to be negative, the angular factor must also be negative. This means that θ must be greater than $\pi/2$, and the z axis must be directed downward. On the other hand, if the $\chi^{(2)}$ element is positive, then θ would be less than $\pi/2$, and the molecular z axis would be oriented up.

Absolute Orientation of Some Organic Molecules at the Air/Water Interface

To obtain the phase of $\chi^{(2)}$, an interference method (20–22) was first used on the phenol/water interface (20), where it was found that the hydroxy end points toward the bulk water (Figure 1). This is understandably the preferred direction, because the hydrogen bonding with the water subphase and the hydrophobic phenyl ring extending into the vapor phase is the lower energy orientation. When bromine was substituted into the position para to the hydroxy group in phenol, thus yielding p-bromophenol, the direction of the permanent dipole moment is reversed and points toward the more positive hydroxy end of the molecule. Measurement of the phase of p-bromophenol showed that the hydroxy end, as with the phenol, is

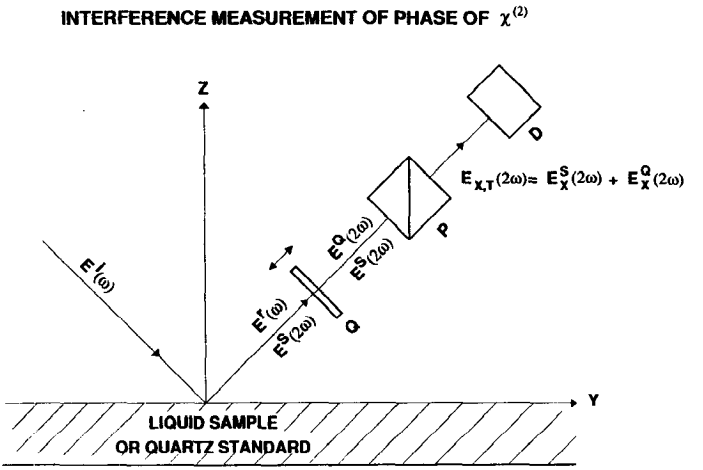

Figure 1 Phase measurement of $\chi^{(2)}$. Q = reference quartz; P = analyzer; D = detector. E^i and E^r are incident and reflected field amplitude at ω; E^s and E^Q are SH fields generated by sample (or quartz standard) and reference quartz Q; E_x^s, E_x^Q, and $E_{x,T}$ are the x components of SH field due to sample, quartz reference and their sum (20).

directed toward the bulk phase (J. M. Hicks et al, in preparation). When a nitro group was substituted para to the hydroxy group yielding PNP, the permanent dipole is again opposite to that of phenol. The phase measurement again indicated that the hydroxy group was dominant in determining the absolute orientation of the molecule, and the hydroxy pointed toward the bulk water. Hicks et al (in preparation) therefore concluded that hydrogen bonding of the hydroxy groups was the determining factor in the absolute orientation, and not the permanent dipole moments of the adsorbed molecules. An interesting aspect of the PNP phase measurement was that the SH frequency was resonant with the peak of the first optical transition for the molecule. Hicks et al (in preparation) found that the phase shift was $\pi/2$ with respect to the nonresonant phenol molecules, exactly as predicted by theory.

Absolute Orientation of Water Molecules at the Neat Water/Vapor Interface

Because of the importance of water, there has been a long-standing interest in its absolute orientation at the neat water/vapor interface, i.e. are the protons preferentially oriented up or down at the neat water/vapor interface? Several theoretical studies have favored the protons down orientation (23–29). Experimental studies of the surface potential have not yielded a conclusive answer, because the results obtained are conflicting (30–35). Although the SH phase measurement method is applicable to water, it is necessary to include the two dominant in plane hyperpolarizability elements, $\alpha^{(2)}_{zzz}$ and $\alpha^{(2)}_{zxx}$, where z is the symmetry axis, and xz defines the plane of the water molecule. The presence of two hyperpolarizability elements introduces additional Euler angles to the orientational factor connecting $\chi^{(2)}$ with $\alpha^{(2)}$. Fortunately, these complications can be avoided by using a simple relation derived for the purpose of having only a single molecular angle in the expression relating $\chi^{(2)}$ with $\alpha^{(2)}$ (36):

$$\chi^{(2)}_{zzz} + 2\chi^{(2)}_{zxx} = N_S[\alpha^{(2)}_{zzz} + \alpha^{(2)}_{zxx}] \langle \cos\theta \rangle.$$

From this expression, we see that measurement of the phases of $\chi^{(2)}_{zzz}$ and $\chi^{(2)}_{zxx}$, together with knowledge of the sign of the hyperpolarizability sum $[\alpha^{(2)}_{zzz} + \alpha^{(2)}_{zxx}]$, yields the sign of $\langle \cos\theta \rangle$ and, thus, the direction of the water dipole (36). The sign of the hyperpolarizability sum obtained from electric field-induced SHG (37) in bulk water, together with the measured (36) signs of $\chi^{(2)}$ in the above expression, leads to the conclusion that the preferred orientation of water at the neat water/vapor interface has the z axis (direction of the permanent dipole moment) pointing toward the bulk water. In this preferred orientation, the oxygen points toward the vapor phase, and the protons point toward the bulk water.

Energetics of Water Orientation at the Neat Water/Vapor Interface

Preferred absolute orientation, or polar alignment, indicates that there are more water molecules with their permanent dipole moments pointed down than up. The phase measurement does not reveal how many more are down versus up or their relative number. The up-down population ratio is determined by the energy difference between a water molecule oriented up versus one that is down, which in turn determines the preferred absolute orientation. From measurements of the strong temperature dependence of the SH signal, Goh & Eisenthal (38) inferred that there is a significant degree of structure at the water interface at room temperature. The observed decrease in the SH signal with increasing temperature was attributed to a decrease in the down versus up orientational populations. The temperature dependence showed a strongly diminishing component with temperature that was attributed to a weakening of the hydrogen bonding orientation forces. The slower diminution at higher temperatures ($> 50°C$) was attributed to electrostatic forces, such as the orientation effects of the permanent water moments. Using a simple model, the up versus down orientation energy was estimated to be $\sim(1/2kT)$ at room temperature. This relatively small energy difference suggests that there is a significant population of water molecules oriented both up and down, which is consistent with the relatively weak SH signal obtained at the neat water/vapor interface.

Absolute Orientation of Molecular Chromophores from SFG

As with measurements of the phase of the SH nonlinear susceptibility $\chi^{(2)}_{SH}$, measurements of the phase of the SF nonlinear susceptibility $\chi^{(2)}_{SF}$ can be used to yield the absolute orientation of the molecule. The measurement of the SF phase yields the absolute orientation of the $\chi^{(2)}_{SF}$, which corresponds to the vibration that is in resonance. This has the attractive feature of providing the absolute orientation of a chromophore on the molecule. The chromophore vibration must be infrared and Raman active to yield an SF signal. Using infrared-visible SFG, Superfine et al (39) measured the phase of $\chi^{(2)}_{SF}$ of the terminal methyl group on pentadecanoic acid ($C_{14}H_{29}COOH$) at the air/water interface. The authors spread the pentadecanoic acid monolayer on an oriented crystalline quartz substrate and used a variation of the interference method to obtain the phase of $\chi^{(2)}_{SF}$. Because the carboxyl group binds to the quartz substrate, the terminal methyl is oriented away from the substrate. By comparing the phase of $\chi^{(2)}$ of the methyl group at the air/water interface with that on quartz,

Superfine et al (39) demonstrated that the terminal methyl group points away from the bulk water at the air/water interface. With this same method, they obtained the phase of $\chi^{(2)}_{SF}$ of the terminal methyl group in a liquid crystal monolayer spread on crystalline quartz. The relative phases of the pentadecanoic acid methyl and the liquid crystal were the same. Because the terminal methyl group of pentadecanoic acid can be confidently assigned to an orientation pointing away from the quartz substrate, the same orientation for the liquid crystal terminal methyl can be inferred from its phase relative to pentadecanoic acid.

In other SF experiments on the methyl vibrations of methanol (CH_3OH) at the neat methanol/vapor interface, Superfine et al (40) found that its phase was the same as that of a methoxy (CH_3O) monolayer adsorbed on glass. Because the methyl group of methoxy points toward the vapor, the oxygen binding to the glass, the authors concluded that the methanol is oriented at the neat methanol/vapor interface with the methyl group pointing away from the liquid. An interesting aspect of the neat methanol interface study was that the orientational distribution was very broad ($\Delta\theta \sim 100°$), based on a fitting that assumed a Gaussian orientational distribution.

Bacteriorhodopsin Chromophore in a Biological Membrane

The absorption of light by the retinal chromophore of bacteriorhodopsin has the physiological result of creating a proton gradient across the bacterial cell membrane. The change in the retinal charge distribution can effect changes in the charge distribution in the surrounding protein, which in turn can alter the potential gradient across the cell membrane. Therefore, it would be important to know which way the retinal chromophore is oriented in the cell membrane. Huang & Lewis (41) addressed this problem by using the SH interference method to measure the phase of $\chi^{(2)}$ of the retinal chromophore of bacteriorhodopsin imbedded in a purple membrane film. They found that the ring part of retinal (β-ionone) pointed toward the extracellular side of the membrane (Figure 2).

LANGMUIR-BLODGETT FILMS

Langmuir-Blodgett (LB) films have attracted a lot of attention because of their potential application in microelectronic and optical technologies. They are readily prepared by transferring a monolayer at a time of a long-chain organic amphiphile from an air/water interface to a solid substrate. The control of the multilayer structure, e.g. by varying the composition of each monolayer, is essential to the control of the LB film's optical and electronic properties. To do this effectively, one needs a microscopic

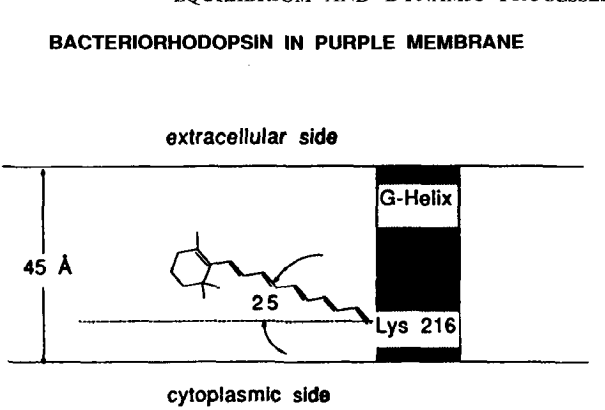

Figure 2 *Trans* orientation of the bound retinal chromophore of bacteriorhodopsin in purple membrane (41).

characterization of the film. Second harmonic generation is proving to be a useful technique for investigating the orientational structure and dynamic effects as functions of the multilayer sequence and composition of LB films.

Because the actual arrangement of molecules in a given monolayer, with respect to molecules in the adjacent layers, can sometimes change from one configuration to another, e.g. head-head to head-tail, subsequent to the deposition, it is necessary to check on the actual structure (Figure 3). To determine the absolute orientation of a hemicyanine monolayer sandwiched between SH inactive monolayers, Sato et al (42) used a modified interference method. The method utilized the SH signal generated from standard molecules on the backside of a silica substrate to interfere

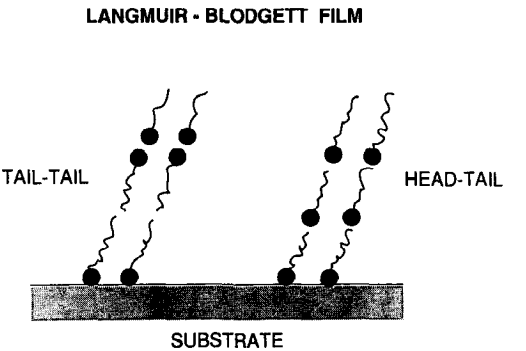

Figure 3 Relative orientations, head-tail and tail-tail, or head-head of long-chain molecules in a LB film.

with the SH signal from the LB film deposited on the front surface. From the fringe pattern, the authors obtained the relative phase of $\chi^{(2)}$, which yielded the absolute orientation of the molecules in the LB film. They found that a Z-type structure (head-tail) of the hemicyanine layer was easily achieved and remained stable in the LB film. Earlier studies of the two cyanine dyes, merocyanine and hemicyanine, in alternating and nonalternating layers used SHG to probe the structure (43). The effects of multilayer structure and the observed SH enhancement proved to be important in developing desired LB films.

Hsiung et al (44) recently studied the effects of modifying the alkane chain by replacing the hydrogens with fluorine to produce novel LB films. The authors found that the fluorinated side groups, which increase the hydrophobicity, stiffness, and chain cross-section, caused significant polar ordering of the monolayers. If the monolayers were randomly oriented with respect to the SH active constituent molecules, the SH signal would be either very weak or nonexistent. In a photochemical study of the perfluorinated LB film discussed above, Hsiung (45) used an ultraviolet (UV) laser to generate a SH grating. With the aid of SH detection, the kinetics of the photobleaching process were obtained (Figure 4). The LB film contained alternating layers of two different polymers, one being SH active and the other not. The UV laser photochemically destroyed a charge

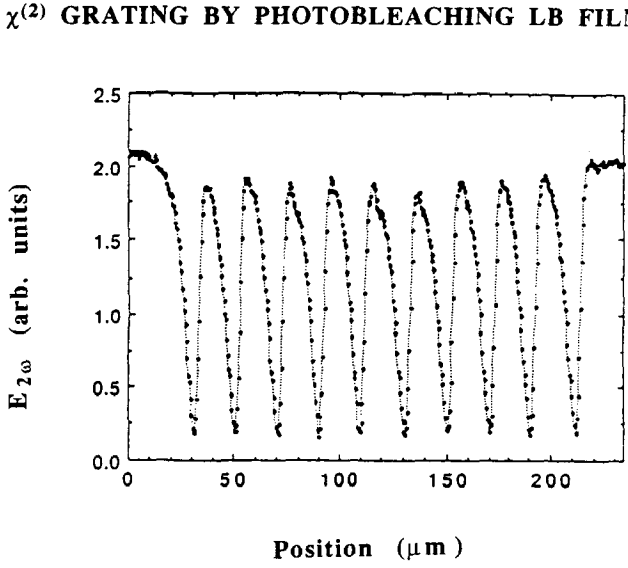

Figure 4 SHG scan of a $\chi^{(2)}$ grating consisting of ten photobleached lines written in a 20-bilayer LB film (45).

transfer chromophore thought to be responsible for the SH signal. The decay kinetics of the SH electric field was first order with the decay constant, depending linearly on the energy flux, the UV absorption cross-section, and the photochemical reaction yield. Under the conditions of the experiment, $I_{UV} = 4.3$ watts/cm^2, the $1/e$ decay required about eight minutes of exposure.

INTERFACE ANALYTICAL CHEMISTRY

The SH and SF methods are valuable, because they can provide quantitative information on the density of chemical species at interfaces. Sum frequency generation is of particular interest, because it is a vibrationally sensitive technique that can differentiate among and identify the various species present at the interface. For interface studies, SFG provides the significant analytical capabilities that one associates with infrared spectroscopy. An excellent demonstration of this, Bain et al (46) studied mixed monolayers of octadecanethiol and its deuterated derivative, octadecanethiol-d_{37}, adsorbed on silver and gold substrates. The SF spectrum in the region of the methyl (CH_3) stretching modes was obtained. The authors showed that a term related to the resonant nonlinear susceptibility, $\chi_R^{(2)}$, obtained from the SF spectra, is directly proportional to the adsorbate surface density. Interestingly, the nonresonant background $\chi_{NR}^{(2)}$, though affecting the lineshapes, does not interfere with analyzing the SF spectra. If anything, the nonresonant background, $\chi_{NR}^{(2)}$ is valuable as a reference for comparing different examples.

Second harmonic generation can also be used as a diagnostic tool of the species present at surfaces. Anderson & Hamilton (47) used SHG to study the effects of high temperatures on the surface properties of materials, such as a single crystal of Fe-18Cr-3Mo, a stainless steel-like alloy. They observed that the effect of exposure to high temperatures resulted in an increase in the atomic fractions of nitrogen impurity and chromium, possibly in the form of a nitrogen-carbon compound at the surface. By comparing the SHG data with Auger results, the authors verified that the surface nonlinear susceptibility, $\chi^{(2)}$, obtained with 700 nm input light, scaled with the chromium and nitrogen surface densities. An interesting result was the observed dependence of the SH signal on wavelength. At 532 nm, the SH signal was far less sensitive to the Cr/N fraction at the surface, but very sensitive to CO adsorbed on the surface. In contrast, the adsorption of CO had only a small effect on the SH signal generated with the 700 nm probe light. This strong wavelength dependence indicates that resonant denominators caused by the various electronic transitions involving surface and other electronic states, modified by molecular and atomic surface species, are important in this system. The resonant con-

tributions are responsible for the high sensitivity of SHG to the population and identity of the surface species.

Despite the frequently observed correlation of $\chi^{(2)}$ with surface coverage, one must be careful in assuming that this is automatically the case. A convincing example of the need for caution is a SH study (48) of CO adsorbed on a Ni(110) surface. The authors found that although some of the measured $\chi^{(2)}$ elements scaled linearly with CO coverage, others did not. An appealing physical picture, in which one set of the $\chi^{(2)}$ elements is dominated by contributions from localized electrons and the other from nearly free electrons, is presented as an explanation. As the CO coverage increases, the interactions between CO adsorbates affect those $\chi^{(2)}$ elements that are sensitive to the localized electron contributors and are responsible for the observed nonlinear coverage dependence. The other $\chi^{(2)}$ elements, which are dependent on the nearly free electrons, experience a linear decrease with CO coverage, as the nearly free electrons are localized by the CO adsorbed.

CHEMICAL REACTIONS AT INTERFACES

As noted earlier, the asymmetry in forces exerted on molecules in the interfacial region affects the chemical composition, polarity, and structure of the interface. Therefore, interfacial chemical reactions, rates, and chemical equilibria will differ from bulk media. We consider the few examples to date of chemical studies at interfaces that use SHG and SFG. One of the areas addresses what is perhaps the most important type of chemical reaction: acid-base reactions. A second example, important in catalysis, deals with the utility of SFG to probe a chemical reaction of an organic molecule, methanol (CH_3OH), on a Ni(100) surface at high vacuum. The last example is a unimolecular chemical reaction involving the isomerization of molecules in excited electronic states.

Acid-Base Reactions at the Air/Water Interface: Charges at Interfaces

To study the acid-base equilibria between p-nitrophenol (HA) and its anion (A^-), Bhattacharyya et al (49) measured the SH intensity generated at the air/solution interface as a function of bulk pH.

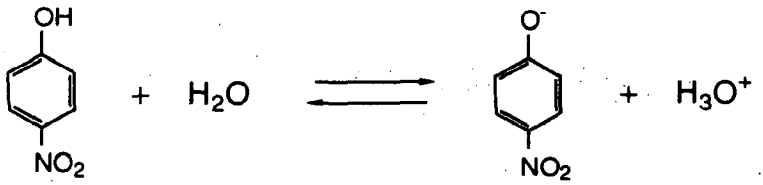

At low pH, where the acidic form HA dominates, the SH signal was roughly a factor of 100 greater than that of neat water. However, as the bulk pH was increased, the SH signal dropped. It continued to drop until bulk pH values in excess of 11 were achieved, at which point the SH signal leveled off to a value equal to that of neat water. Although the bulk solution at high pH is predominantly nitrophenolate, these results show that nitrophenolate is not present in the interfacial region; if it were, it would generate a signal much larger than that of neat water. The acid-base equilibrium of p-nitrophenol is shifted at the surface toward the neutral form, because the charged nitrophenolate ions are more stable in the bulk polar medium than at the air/water interface, where they are repelled by image forces.

How then does one study acid-base equilibria at an air/water interface in a quantitative fashion, as it is necessary to have both the neutral and the charged forms present? The answer is to stabilize the charged form at the interface, which can be accomplished by attaching hydrophobic groups to the molecule. This method has the effect of lowering the adsorption free energy. To quantify the adsorption process, Castro et al (50) studied the energetics of adsorption for the neutral and charged forms of the acid phenol (C_6H_5OH) and the base aniline ($C_6H_5NH_2$) by attaching a hydrocarbon chain to the para position. At high pH for the phenol derivative, the bulk solution consists overwhelmingly of the charged form (phenolate) CH_3–$(CH_2)_n$–$C_6H_4O^-$. In other experiments on aniline derivatives carried out at low pH, the charged aniline form (anilinium) CH_3–$(CH_2)_n$–$C_6H_4NH_3^+$ dominates in the bulk solution. For both cases, when the alkyl chain has five or more carbons ($n \geq 4$), the hydrophobic forces, which drive the molecule to the interface, overcome the repulsion and solvation forces, which then drive the molecules into the bulk solution. The result is an increase of the SH signal above that of neat water (Figure 5).

The adsorption isotherms were obtained from measurements of the SH signal as a function of the bulk concentration of the phenolate ions in one case and the anilinium ions in the other. The adsorption isotherms for these charged molecules were in excellent agreement with a Langmuir adsorption model and yielded the free energies of adsorption, ΔG^0_{Ads}. The ΔG^0_{Ads} for the charged species can be broken down into a chemical part, ΔG^0_{Chem}, and an electrostatic part, ΔG^0_{El}, associated with the formation of the charged double layer at the interface (1):

$$\Delta G^0_{\text{Ads}} = \Delta G^0_{\text{Chem}} + \Delta G^0_{\text{El}}.$$

This electrostatic free energy is related to the electrostatic interface potential Ψ_0,

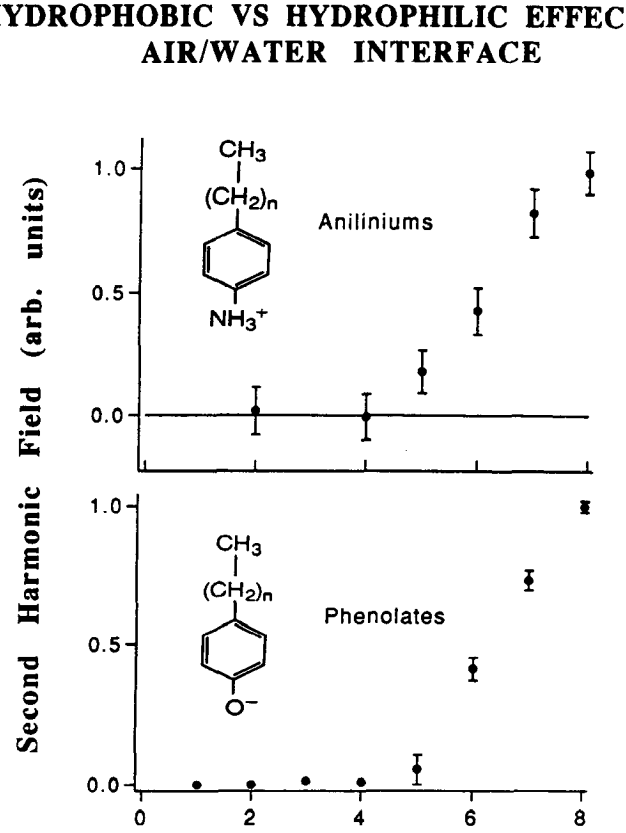

Figure 5 SH field as a function of carbon chain length for phenolate and anilinium ions (50).

$$\Delta G^0_{El} = N_A z e \Psi_0,$$

where N_A is Avogadro's number and z is the ion valency. From a determination of the charged species population at the surface in conjunction with the Guoy-Chapman model of the double layer (1), the value of Ψ_0 can be obtained. These SH experiments yielded the free energies of adsorption, the quantitative effects of an additional CH_2 group on the adsorption free energy ($\sim$800 cal/mole), and the interface pH as a function of the interface charge density (50). The interface pH_s is obtained by using the Boltzmann equation, which relates the interface pH_s to the bulk pH_B and the interface potential,

$$pH_s = pH_B + e\frac{\Psi_0}{2.3kT}.$$

Obtaining the surface pH is a necessary step in the determination of the acid-base equilibrium at an interface:

$$HA + H_2O \overset{Ka}{\rightleftharpoons} A^- + H_3O^+.$$

The equilibrium pK_a at the interface can be written as,

$$pK_a^s = pH_s + \log(HA)/(A^-).$$

For the aniline system, the acid form HA is the charged form CH_3–$(CH_2)_n$–$C_6H_4NH_3^+$. The pK_a^s of $C_{16}H_{33}$–C_6H_4–NH_3^+ was 3.6 ± 0.2 at a total electrolyte concentration of 1 M. The bulk pK_a is 5.3, which shows that the acidity of the anilinium increased by a factor of 50 with respect to the bulk aqueous solution. The anilinium acid-base equilibrium is shifted toward the energetically more favorable neutral form at the interface. In contrast to the anilinium case, the pK_a^s of phenol $C_{18}H_{37}$–C_6H_4OH increased at the surface, from 10 in the bulk to 12 in the interface. The decrease in acidity of the phenol derivative is caused by the lower free energy of the neutral acidic form HA, just as the increase in acidity of the anilinium derivative is caused by the higher free energy of the charged acidic form HA^+.

In another study of acid-base equilibria, Xiao et al (51) used the SH method to determine the pK_a^s of a hemicyanine molecule imbedded in a negatively charged monolayer of stearic acid. This is in contrast to the previously discussed experiments, in which the charged interface was formed by the acidic or basic forms of the molecules studied. The pK_a value of the hemicyanine dye acid-base equilibria

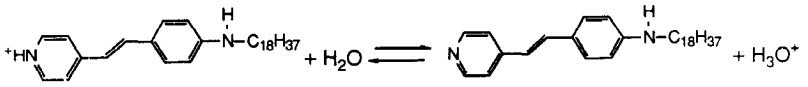

was 3.5, compared with the bulk value of 6.7. The very large increase in acidity at the interface is primarily caused by the very high density of positive charge of the ionized stearic acid monolayer and, to a lesser extent, the repulsion of charges from an air/water interface.

Methanol Adsorption and Reactions on Ni(100)

At a low temperature (100 K), molecular methanol is stably adsorbed to the Ni(100) surface by using its oxygen nonbonding electrons to bond with

the Ni surface. The adsorption has been observed by using SHG (52) and SFG (53) of the methanol methyl vibrational stretches. On raising the surface temperature into the range of 160–210 K, the methanol decomposes by breaking the OH bond to produce methoxy (CH_3O) plus a surface hydrogen atom. The decomposition to CH_3O is seen in the change in the SH signal and, more specifically, in the SF spectrum of the methyl vibrations, where a marked change in the lineshapes and a 10 cm^{-1} shift to higher frequency occurs. The change in lineshape is associated with the breaking of the OH bond of methanol, which in turn affects the interference between the resonant and nonresonant components of $\chi^{(2)}$. The further heating of the surface to 256 K results in the decomposition of methoxy to CO and three hydrogen atoms (Figure 6). From the temperature dependence and the kinetics of the decay monitored by SHG, an activation energy of 17 kcal/mole and an Arrhenius factor of $10^{12.4}$ is obtained. A very pronounced, but as yet not understood, effect is the reduction in reaction rate, as monitored by SHG (52), upon the addition of sulfur at a surface coverage of 1–4%. From the SF studies, the decomposition of methoxy is manifested by the disappearance of the methyl stretches. Although one might have expected to observe the C–O vibration upon the decomposition of methoxy, it was not observed in scans down to 1850 cm^{-1}. After desorbing the H atoms produced in the methoxy decomposition, the CO vibration was observed. Apparently, the presence of H atoms shifts the CO frequency to below 1850 cm^{-1}.

Photoisomerization of an Organic Molecule at the Air/Water Interface

The structural change (isomerization) of a molecule in an excited electronic state is an example of a unimolecular chemical reaction. In bulk solution, the intramolecular motions associated with the isomerization are usually sensitive to the friction experienced by the reactive coordinate in its motion

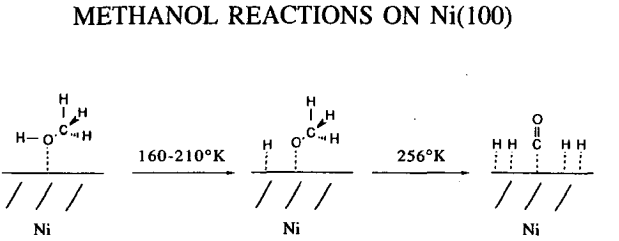

Figure 6 Thermal reactions of methanol on Ni(100) (53).

on the reaction potential surface. In addition to the friction, which in some cases can be directly related to the solvent viscosity, the solvent polarity can be important in changing the reaction potential surface, e.g. its slope and energy barrier. Numerous experimental and theoretical studies of photoisomerizations in solution have attempted to understand the role of the solvent in these prototypically "simple" chemical reactions better. To date, there have only been a few photoisomerization studies at interfaces.

In one series of studies, Meech & Yoshihara (54, 55) compared the photoisomerization dynamics of the dye malachite green adsorbed at an air/quartz interface with the dynamics at a liquid (diethyl ether)/quartz interface. The authors excited the adsorbate molecules with a pump pulse and, with a time-delayed probe pulse, measured the SH signal. The SH signal depends on the populations, nonlinear polarizabilities, and their relative phases, of the ground and excited state molecules at the measurement time. The isomerization kinetics was the same within experimental error, 40 ps, at both interfaces. This result was somewhat surprising, because malachite green, as with other triphenylmethane dyes, undergoes a barrierless isomerization, at least in solution, thus resulting in a rapid ground state recovery. The isomerization in solution is strongly affected by the solvent viscosity. This is clearly not the case at the air/quartz or liquid/quartz interfaces. Furthermore, the isomerization is much slower at the interfaces than at the bulk liquid.

In contrast, the dye molecule DBI [2-(p-dimethylamino)styrl)-1-ethyl-bernzothiazolyl iodide] undergoes a somewhat more rapid isomerization about its central double bond at the air/quartz interface (43 ps) than in the bulk ethanol solution (55 ps) (55). From the studies of the solid interface isomerizations, the details of the solid-adsorbate interactions are apparently crucial in the dynamics, especially of malachite green. Unlike isomerizations at solid interfaces, SH studies have found that the dye DODCI (3,3′-diethyloxadicarbocyanine iodide), which undergoes a *cis-trans* isomerization about one of its double bonds, is significantly faster at the air/water interface (220 ps) than in bulk water (520 ps) (56). This is consistent with the lower friction at the air/water interface versus the bulk water. At an air/water interface, it is not clear whether the reaction potential is significantly different than in the bulk solution. If the reaction involves a significant change in charge distribution, then the difference between interface and bulk polarity could result in different isomerization potential surfaces. Also, the difference in the interface versus bulk friction is expected to be an important factor in the isomerization dynamics.

DYNAMIC PROCESSES AT INTERFACES

Because of the unique chemical composition, orientational structure, and asymmetry in the forces exerted on molecules at interfaces, just as with equilibrium properties, the dynamics of molecular phenomena differ from their bulk counterparts. We have already discussed interfacial effects on the unimolecular chemical reaction of excited state isomerization. We now consider other examples of interface dynamics.

Intermolecular Electronic Energy Transfer

The transfer of electronic energy among molecules that comprise the molecularly thin sheet of an interface is important to the photochemistry and photophysics at interfaces. In an interfacial energy transfer experiment at the air/water interface, Sitzmann & Eisenthal (57) used rhodamine 6G as the excited donor and DODCI as the ground state acceptor. The authors selectively pumped a submonolayer of rhodamine 6G and monitored the effect of the DODCI acceptor on the rhodamine 6G lifetime by measuring the kinetics with SHG as a probe. The bulk concentrations of donor and acceptor were kept low, so that the bulk donor-acceptor distance was large ($\sim$130 Å). In the absence of acceptor, the rhodamine 6G lifetime at the interface was 3.1 ns. This value is not very different from a bulk value of 3.7 ns, which indicates that there is not significant dimer formation or excited rhodamine 6G to ground rhodamine 6G interface energy transfer. [When the rhodamine 6G adsorbate density is high, as in SH experiments (54) carried out at a solid (quartz)/water interface, a rapid decay (100 ps) of the rhodamine 6G excited state was observed. Under these conditions, the effects of dimer trapping and/or energy transfer were thought to be of dominant importance.] In the presence of ground state DODCI, with which the fluorescence from excited rhodamine 6G has a large spectral overlap, the lifetime of the rhodamine 6G at the air/water interface decreased by a factor of three to 1 ns. In the bulk region of the same solution, the fluorescent lifetime of rhodamine 6G decreased by only about 15%. The origin of these differences is the strong adsorption of DODCI to the interface, which results in much smaller donor-acceptor distances than in the bulk solution; thus, a larger donor-acceptor transfer rate occurs at the interface. Possible effects of dimensionality (two at the interface versus three in the bulk) on the observed kinetics were also examined (57). Although the two-dimensional fit is possibly better than the three-dimensional fit, the results are not conclusive, and further investigation is required.

Rotational Motions at the Air/Water Interface

The orientational relaxation of molecules in bulk liquids (58–60) and restricted environments (61–63) are active areas of research that probe

molecular forces in bulk liquids, membranes, micelles, and vesicles. At liquid interfaces, the study of rotational molecular motions has been limited to fluorescent probes covalently attached to an insoluble long-chain lipid, thereby avoiding any overwhelming fluorescence from a large bulk probe population (64). With SHG, one can selectively investigate the rotational motions of molecules at an interface, even when they have a large population present in the bulk liquid. Furthermore, the adsorbed molecules are not hindered in their motions by any covalent attachment to a long-chain lipid.

Castro et al (65) disturbed the equilibrium orientational distribution of rhodamine 6G molecules by photoselective excitation with a polarized picosecond laser pulse (Figure 7). They monitored the relaxation of the perturbed orientational distribution by observing the SH signal from a time-delayed probe pulse. The SH signal changes markedly on excitation, because of the difference in ground and excited state nonlinear polarizabilities. It continues to change in time, as the ground and excited molecules rotate toward their respective equilibrium orientations and as the excited molecules relax to the ground state. At the low concentrations used, there was no change observed in the rotational dynamics upon doubling the rhodamine 6G concentration. This result indicates that energy transfer and dimerization effects were not significant. The authors

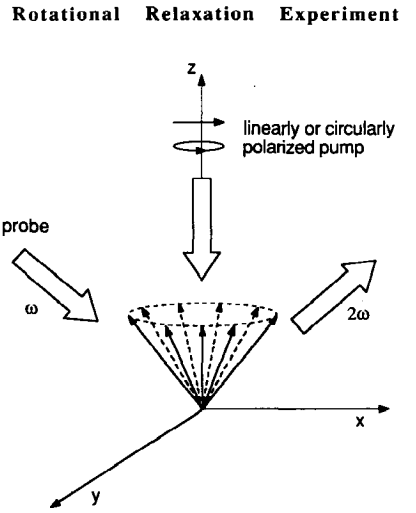

Figure 7 Pump-probe experimental setup. Arrows represent transition dipoles arranged to a common origin. Pump beam disturbs equilibrium orientational distribution at interface. Relaxation is monitored by SH signal (2ω) generated by a time-delayed probe (ω) (65).

proved that the observed dynamics was polarization dependent by demonstrating that different nonlinear susceptibility elements obeyed different kinetics. In other words, the measured kinetics changed when either the polarization of the incident probe pulse or the analyzer setting for the SH signal were changed. For example, one element, $\chi^{(2)}_{xzx}$, continued to decrease after photoexcitation, whereas a different element, $\chi^{(2)}_{zxx}$, increased (Figure 8). The time scale of the rotations appears to be in the range of several hundred picoseconds to a nanosecond, but a model for the rotation is necessary to extract specific orientational rate constants. The rotation of rhodamine 6G might appear to be slower than bulk water (58), but because different orientational moments are being probed and the decay may not be simple exponential, one must be careful in comparing the kinetic curves.

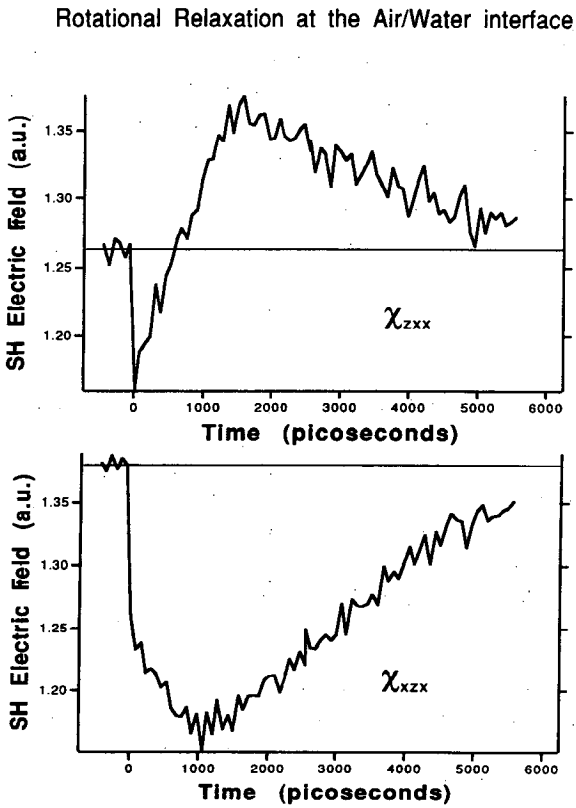

Figure 8 Relaxation kinetics of the $\chi^{(2)}_{zxx}$ and $\chi^{(2)}_{xzx}$ nonlinear susceptibility elements of the SH signal from the interface of a rhodamine 6G aqueous solution (65).

In addition to the time scale of interface rotational motions, the amplitude of the SH signal increased with rotation beyond its initial ground state value. This observation was interpreted in terms of the difference between the equilibrium orientation of the excited versus ground state molecules, because of the change in excited state dipole moment and general charge distribution, which could directly affect the orientation of a molecule at the air/water interface. As seen in experiments using linearly polarized and circularly polarized pump pulses, the rotational relaxation was dominated by out of plane molecular motions (58).

Surface Diffusion of Hydrogen Atoms on Si(111)

Although the lateral motion of adsorbates on the surface of a solid is important in determining the chemical and physical properties of a surface, there are only a few direct studies (66). Most information is obtained indirectly from crystal growth studies, in which lateral diffusion plays a key role (67). A direct approach with SHG has been used to study the diffusion of chemisorbed hydrogen atoms on the Si(111) 7×7 surface (68). The method involved the creation of a hydrogen concentration grating by a laser-induced desorption of the H atoms, as was first done for CO on Ni(111) (69). The decay of the grating caused by surface diffusion was monitored by measuring the diffraction at the SH frequency of a time-delayed probe beam. The diffusion was observed over an estimated length of about 1000 Å with a barrier to lateral motions of 1.5 eV, which is roughly one half of the binding energy of atomic hydrogen on Si. This barrier is larger on Si than on metals, where the lateral motion is faster.

Dynamics of Molecular Adsorption to the Surface of a Liquid Jet

The air/liquid jet interface that is created when a liquid exits from a jet nozzle has the effect of generating nonequilibrium interfacial populations. For example, the population density of solute molecules, such as nitrophenol at an air/water jet interface immediately after the nozzle, is determined by the interactions of nitrophenol at the preceding nozzle/aqueous solution interface and the liquid motions involved in the formation of the jet, not by nitrophenol interactions at the later developing air/water jet interface. Thus, the air/water jet interface initially has an interface density of nitrophenol molecules that is not its equilibrium air/water population. By measuring the SH signal at various positions along the axis of the water jet, Castro et al (70) measured the time-dependent change in the interface nitrophenol population. The adsorption kinetics fitted a time-dependent Langmuir model. The rate constant for adsorption was $(4.4 \pm 0.2) \times 10^4$ s^{-1}; for desorption, it was 6 ± 2 s^{-1}. The free energy of adsorption, which

was calculated by using these rate constants, was 5.1 kcal/mole. This value is the same as that obtained from an equilibrium measurement at a static air/aqueous nitrophenol solution interface (70). This agreement supports the validity of the kinetic model used, because the adsorption free energy must be the same, whether obtained from equilibrium or dynamic experiments. The authors also concluded that the adsorption kinetics was not diffusive and considerably slower than diffusion controlled, which indicated that the adsorption kinetics was controlled by an activation barrier to adsorption estimated to be a few kcal/mole. The possibilities of using jets or moving interfaces to study dynamic processes, as well as using them to avoid irreversible photochemical and thermal processes, appear promising.

Diffusion and SH Fluctuation Spectroscopy

An interface prepared by spreading long-chain lipids on water can be described by the way the lipid molecules self-arrange. If the density of lipids is low enough that lipid-lipid interactions can be neglected, then a gas-like equation of state involving the surface pressure, area per lipid molecule, and temperature is obtained. If the density is sufficiently high, then a liquid-like phase occurs. Under appropriate conditions, a coexistence between these two phases can occur, i.e. clusters of liquid density interspersed with individual gas-like lipid molecules. Therefore, the surface is not a homogeneous liquid phase or gas phase, but is heterogeneous. Second harmonic experiments on fatty acids and aromatic head group lipids have shown that this method can be used to investigate the equilibrium and dynamic properties of heterogeneous interfaces (71–73). By irradiating a sufficiently small area of the surface with a focused beam (~ 10 μm), Zhao et al (72) could observe fluctuations in the SH intensity, which were caused by the variation in time of the number of clusters occupying the irradiated area. The time scale of the fluctuations is determined by how rapidly the clusters diffuse in and out of the observed area. In the coexistence region, the fluctuations are not Poisson distributed; in the homogeneous liquid region, they conform to the expected Poisson distribution. From measurements of the time autocorrelation function of the SH intensity, the average diffusion constant was approximately 10^{-8} cm^2/s, which indicates that the friction is low. The average size of a cluster was an estimated ~ 1 μm, based on the fit of the data to a diffusion model (Zhao et al, in preparation). From the constancy of experimental results taken over a long period of time (~ 1 day) and from the results on interfaces having the same average lipid density, but prepared differently, Zhao et al concluded that the observed fluctuations were not caused by the breakup and formation of clusters. Rather, they were caused by the metastable, but

very long lived, clusters thermally diffusing into and out of the observed region of the interface.

Recombination Kinetics and Desorption of H_2 from Si(111)

A variety of methods, such as temperature-programmed desorption (TPD) and laser-induced thermal desorption (LITD), have been used to investigate the bonding and reaction kinetics of chemisorbed species on semiconductor surfaces. The effect of hydrogen on silicon is particularly interesting. At low coverages, a single hydrogen atom bonds to a silicon atom yielding Si–H; at higher coverages, other hydride species Si_xH_y may be present. One important issue is the reaction kinetics for the recombination of hydrogen atoms, which results in the desorption of H_2 from the Si surface. The very high sensitivity of SHG to the adsorbed hydrogen makes it possible to study the kinetics down to a 0.01 monolayer coverage (74). The SH studies of the desorption kinetics of hydrogen from the Si(111) 7×7 surface found that the reaction for the recombination was between first and second order. Various TDP and LITD studies obtained reaction orders that were either first or second order (75, 76). The SH technique made it possible to study the kinetics for sufficiently low coverages, where the monohybride Si-H species is the dominant one, and to demonstrate that the desorption kinetics do not obey the second order kinetics expected for a simple recombination reaction. A simple model that describes the reaction in terms of a thermally activated recombination and two binding sites with different binding energies and reaction rates was consistent with the data (74).

VIBRATIONAL RELAXATION AT SOLID INTERFACES

The dynamics and pathways by which vibrationally excited adsorbates dissipate their excess energy is important to any description of surface chemistry, surface diffusion, and surface desorption processes. The decay mechanisms, whether energy transfer to the substrate or intramolecular redistribution, provide insight into the nature of the adsorbate-substrate interactions. The infrared pump and the SF probe technique have made it possible to investigate adsorbate vibrational relaxations at planar and, in some cases, well-defined crystalline substrate surfaces (77). This is in contrast to a large area amorphous silica sample, in which some excellent work was carried out with an infrared pump and infrared probe technique to study the -OH vibrational relaxation (78). With either method, information on the population decay can be obtained; however, such information cannot be obtained from line width measurements of surface

vibrations, unless the pure dephasing contributions can be neglected. The SF method involves the measurement of the change in population of a vibrational mode, pumped by an infrared picosecond pulse and probed by the generation of a SF signal, by using a pair of visible plus infrared pulses. The time profile of the population decay is achieved by varying the time separation between the pump infrared and probe pulses.

Single Crystal Metal Surface

The first experiment on vibrational energy relaxation at a single crystal metal surface was that of the symmetric C–H stretch (2918 cm^{-1}) of methyl thiolate (CH_3S) on Ag(111) (79, 80). The decays were described as biexponential; the faster decay of ~ 3 ps was temperature independent, whereas the slower decay varied from 55 ps at 380 K to 90 ps at 110 K (Figure 9). Interestingly, energy transfer to the metal substrate was not a dominating decay path. If it had been, the decay would be a single exponential. In fact, neither component involved transfer to the metal, but rather an intramolecular transfer, possibly a C–H bending overtone and an asymmetric CH stretch.

Long Chain Adsorbate on a Metal Film

The energy relaxation of three different CH vibrational modes of the terminal methyl group of a Cd stearate [$Cd–(CH_2)_{16}–CH_3$] monolayer on

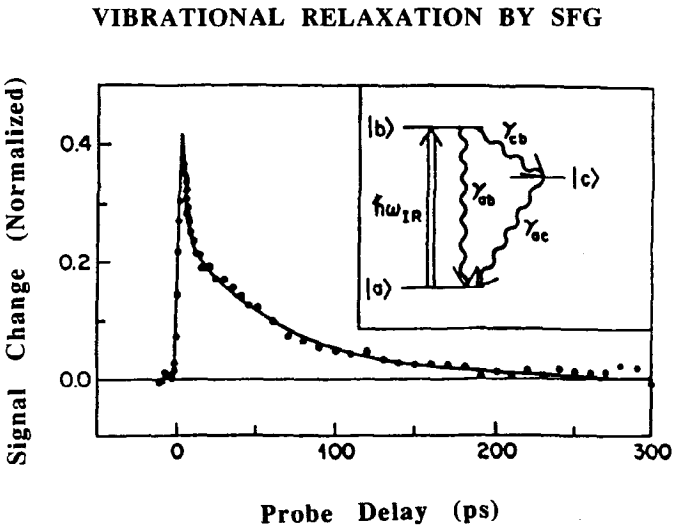

Figure 9 SFG signal from the decay of the symmetric C–H stretching mode of methyl thiolate (CH_3S) on Ag(111). Solid line is the calculation using the three-level population decay model shown in inset (79).

an Ag film were investigated by SFG (77). The decays were were quite different, ranging from a multicomponent (2.5 ps, 165 ps, tail) decay of the symmetric 2878 cm^{-1} CH stretch to 2–3 ps for the other modes. This result is noteworthy: There is not rapid equilibration between the CH modes before decay, which is in contrast to the rapid equilibration that supposedly occurs between the CH modes for hydrocarbons in the liquid phase (81).

Lifetime of an Adsorbate-Substrate Vibrational Mode

The SFG measurement of the lifetime of the Si–H vibration on an H-terminated Si(111) surface constitutes the first measurement of the population lifetime of an adsorbate-substrate vibration (82, 83). The very long lifetime (0.8 ns) of the 2084 cm^{-1} Si–H stretch shows that it is only weakly coupled to the substrate phonons.

Coherence Effects in Pump-Probe SF Experiments

In the analysis of the vibrational decay processes, the effects of coherent processes are generally, and often justifiably, neglected. However, the early time part of the kinetics can be sensitive to both the coherence time of the vibration (T_2) and coherent artifact effects caused by the interactions between the commonly derived infrared pump and infrared probe pulses (84). These latter coherent artifact effects are also encountered in electronic transitions involving visible-visible or UV-UV pump-probe experiments (85). Using a three-vibrational level model, Harris & Rothberg (84) investigated these coherence effects. For methyl thiolate on Ag(111), the fast dynamics was caused by the population decay; for CO/Cu(100) experiments, the vibrational coherence time was an important part of the observed time resolution.

SIGN OF MOLECULAR DIPOLE MOMENT DERIVATIVES FROM SFG

By using a novel application of the measurement of the phase of the SF nonlinear susceptibility for systems in which the absolute molecular orientation is known, we can determine the phase (sign) of the molecular dipole moment derivative $\partial\mu/\partial Q$ (86). Because the measured nonlinear susceptibility, $\chi^{(2)}_{SF}$, is related to the molecular nonlinear polarizability for the SFG, $\alpha^{(2)}_{SF}$, by an average over the molecular orientations, it follows that a measurement of the sign of $\chi^{(2)}_{SF}$, together with the known absolute orientation, will yield the sign of $\alpha^{(2)}_{SF}$. The resonant part of the molecular nonlinear polarizability, $\alpha^{(2)}$, is proportional to the product of the dipole moment derivative, $\partial\mu/\partial Q$, and the linear Raman polarizability derivative,

$\partial\alpha^{(1)}/\partial Q$, with Q being the vibrational normal coordinate. For the C–H stretch of an alkane methyl group, there is good theoretical support for $\partial\alpha^{(1)}/\partial Q$ being positive, i.e. the linear polarizability increases as the C–H bond extends in hydrocarbons, for all molecular orbital hybridizations. For the dipole moment derivative $\partial\mu/\partial Q$, the situation is different. The sign of $\partial\mu/\partial Q$ is expected to change with the bond hybridization and depend on the electronegativity of an attached group X, e.g. X–CH. A SFG phase measurement of the terminal methyl group of a pentadecanoic acid monolayer at the air/water interface demonstrated that $\partial\mu/\partial Q$ is negative, consistent with ab initio calculations (87). For the methyl group of methoxy (CH_3O) bonded by the oxygen to glass, the value of $\partial\mu/\partial Q$ was positive. Although there are no ab initio calculations for comparison, studies of infrared intensities indicate that the dipole moment derivatives become more positive with increasing electronegativity of the substituent X in X–C–H structures, consistent with the SF results (88).

PHASE TRANSITIONS AT INTERFACES

The sensitivity of SHG and SFG to the density and orientational structure of molecules adsorbed to an interface makes them useful as probes of interfacial phase changes (71, 72).

Pyridine on Ag(111)

Haskett et al (89) observed a coverage-dependent phase transformation of pyridine, C_5H_5N, on an Ag(111) surface by using SHG. The change in bonding and orientation obtained from the SH experiments is consistent with UV photoemission and high-resolution electron energy loss studies of the same system (90). Apparently, the pyridine forms π-bonds with the Ag surface in a nearly flat orientation at low coverages. At higher coverages, a new closely packed structure develops. The phase transformation may entail the tilting of the pyridine with the bonding of the pyridine nitrogen lone pair electrons to the Ag surface (89, 90).

Orientational Phase Transitions of Long-Chain Amphiphiles at the Air/Water Interface

It is especially rewarding when a new method yields interesting and unanticipated results. A recent report of orientational fluctuations in the SH signal of hexadecylaniline, $CH_3(CH_2)_{15}C_6N_4NH_2$, is such a case (73). The method used was SH fluctuation spectroscopy, which had provided information on the dynamics of cluster motions in the coexistence region of lipids at the air/water interface (72). At the liquid terminus of the

coexistence region of hexadecylaniline, the large density fluctuations caused by the motion of the clusters into and out of the laser-focused interface area disappeared, and the fluctuations became Poisson distributed, characteristic of a homogeneous surface. However, further compression into the liquid phase region showed the presence of new, strong fluctuations. These fluctuations are orientational (not density) in character, as they depend on the polarizations of the measured incident light and the SH light. These results were unexpected, because the surface pressure-area (π-A) phase diagram showed no evidence of any phase transition in this region. The phenomenon was attributed to an orientational phase transition of the head group, with a strong dependence on chain-chain, as well as dipole-dipole and lipid-water, interactions. Measurements of the SH autocorrelation decay time at different lipid densities (36–28 $Å^2$) and at different areas of laser irradiation (beam radius, 3–6 μm) indicate that the observed phase transition is second order or weak first order.

ELECTROCHEMISTRY: THE METAL/WATER INTERFACE

Origin of the SH Signal

There is considerable interest and activity in the interface electronic properties of a metal surface in contact with an aqueous solution. Studies in electrochemical cells make it possible to modify the metal interface by controlling the electric field at the interface with an external voltage. The importance of the electrode/aqueous interface has been a strong stimulus for the further development and application of SHG and SFG techniques to understand these interfaces better (4). To extract detailed information, it is necessary to determine the source of the measured nonlinearity as a function of the applied potential, the molecules adsorbed, and the surface structure and symmetry. Early SHG studies clearly demonstrated the sensitivity of the observed SH signal to the applied potential (91). Recent SH studies of the Ag(111) electrode/aqueous interface nonlinearity at different potentials have sought to determine the contributions responsible for the nonlinear response (92). The normal component of the surface polarization varied by more than one order of magnitude over the potential range ($\sim$1.5 V) scanned. The data analysis involved calculations that used the jellium model to represent positive charges and a density-functional method to treat surface charge density screening caused by the laser radiation. The agreement of calculations with experimental data was very good. There is also a strong dependence of the SH signal on the wavelength of the incident laser radiation (92–96). Studies of Ag(111), Ag(110), Ag(100), and Au(111) electrodes showed such effects at 1064 nm and 532

nm incident laser wavelengths (92–95). The observed results depend on whether the excitation wavelength was above or below the free electron regime. Excitation above versus below the free electron regime selects different nonlinear susceptibility elements, which depend differently on the applied potential and, consequently, yield a different SH response as the potential is varied. The success of these analyses suggests that the nonlinear response is chiefly caused by the electronic properties of the metal surface; thus, the nonlinearity due to the aqueous electrolyte part of the interface can be neglected in these systems. Although the strong dependence of the SH signal on the applied potential in an electrochemical environment has been extensively demonstrated, the apparent discrepancy reported on the nature of the potential dependence for a silver electrode at 1064 nm highlights some fundamental issues (96, 97). Tadjeddine & Guyot-Sionnest (98) have shown that the apparent disagreement in the SH results was not caused by the surface roughness effects, as had been conjectured, but rather by the difference in excitation geometries that results in different Fresnel factors.

When crystalline metals are used as the electrode material, an additional handle on the metal/aqueous interface can be obtained by rotating the electrode about the normal to the surface. The observed variation in SH intensity on electrode rotation contains information on the symmetry of the surface and the isotropic and anisotropic contributions to the nonlinear susceptibility (4). Results on the rotational anisotropy of the Ag(111)/aqueous interface showed that neither dipole-induced surface states nor oxide impurities on the surface explain the observed behavior (94). In addition, the rotational anisotropy measurements yielded a further interesting result: The SH response of Ag(111) in an electrochemical environment and the Ag(111)/vacuum interface in an ultrahigh vacuum environment are very similar (Figure 10). This suggests a strong similarity in the surface electronic properties and surface structure for the two different interfaces. In using rotation patterns, Lupke et al (99) have theoretically demonstrated that complications interfering with a complete symmetry analysis can occur. As an experimental example of this, a potential-induced reconstruction of an Au(111) surface was discussed.

Adsorption of Atoms and Molecules to the Metal Surface

In addition to the above-mentioned application of rotational anisotropy measurements, the inherent sensitivity of the method to the surface ordering and electronic properties has led to its use in studies of the adsorption of atoms and molecules to metal surfaces. Second harmonic rotational anisotropy studies of the adsorption of atomic iodine and carbon monoxide to a Pt(111) electrode have indicated that either a reduction in surface symmetry occurred or there was an additional anisotropic nonlocal

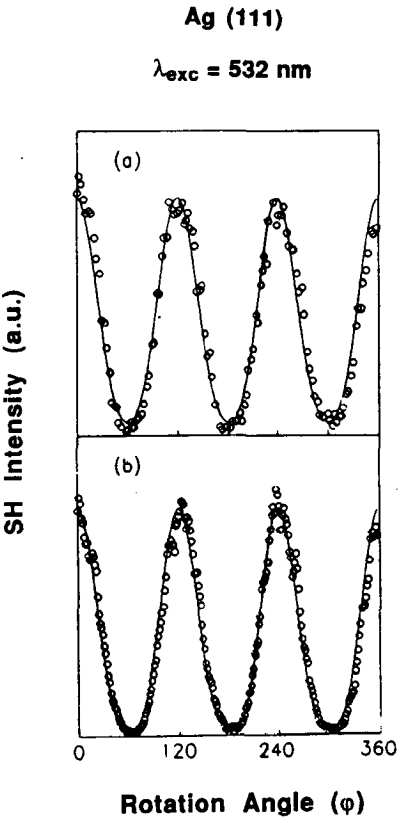

Figure 10 SH rotational anisotropy from Ag(111) (*a*) in ultrahigh vacuum and (*b*) in the electrochemical cell (94).

contribution to the nonlinear susceptibility (100). From rotational anisotropy investigations of the effects of the deposition of thallium and lead atoms on Ag(111) and Ag(110) electrodes, the relative changes in the components of the nonlinear susceptibility were obtained (101). These results were analyzed by using a Langmuir adsorption model and assuming stepwise deposition.

Koos & Richmond (102) have demonstrated a new application of the phase of the SH nonlinear susceptibility, i.e. not to the absolute orientation, in studies of electrode/aqueous interfaces. Using an interference method, they measured the phase changes that occur during the electrochemical deposition of thallium atoms on to an Au(111) electrode. The combination of SH intensity and phase data provides a more complete description of the deposition process. For example, as the second thallium layer is formed,

the measured change in phase is considerably different than that at submonolayer coverages. This phase change, which indicates that the states responsible for the nonlinear susceptibility are considerably different for the first and second layers, is not apparent in the SH intensity data.

A further way to probe the mechanisms for the deposition of foreign atoms onto electrodes is a time-dependent measurement of the SH signal as the deposition proceeds. Robinson & Richmond (103) have obtained important details of the deposition process of thallium atoms onto an Ag electrode by combining SH kinetic data with measurements of the time-dependent cell current. Findings that the deposition is sequential, rather than competitive, at energetically distinct sites, and that it is activation controlled can be obtained by this optical and electrochemical current approach. Information on nucleation and growth can also be obtained.

Campbell et al (104) have observed the electrochemical reduction of a monolayer of the dye of methylene blue adsorbed on a modified crystalline platinum electrode by measurement of the resonant molecular SH signal. A sulfur modified platinum electrode reduces the nonresonant SH signal from the metal surface to a negligible level and prevents the irreversible decomposition of the adsorbed dye. This approach makes both the electrochemical reaction and the molecular orientation of the adsorbate amenable to investigation.

SFG at an Electrode/Water Interface

As noted above, the powerful analytical capabilities of vibrational spectroscopies make them very desirable approaches to molecular phenomena. The first application of SFG to an electrode/aqueous interface demonstrated that the method is, indeed, very promising for electrochemical studies (105). The experiments were carried out on the adsorption of cyanide ion, CN^-, to a platinum electrode. The effect of CN^- on Pt is of some interest, because it poisons the surface and interferes with hydrogen adsorption. The SF spectrum shows the presence of two distinct vibrational bands, whose relative amplitudes are dependent on the applied potential. Based on a line-shape analysis and a SF experiment using thiocyanate ion SCN^-, Guyot-Sionnest & Tadjeddine (105) proposed, in agreement with Ashley et al (106), that the two bands are caused by the two adsorbed orientations of the CN^- on the platinum electrode. One is the carbon bonded CN^- and the other is the antiparallel nitrogen bonded CN^-.

SUMMARY

The level of microscopic information and sophisticated nonlinear spectroscopy experiments on interfaces had made major advances in the past

several years. The range of possibilities for studying physicochemical and biological interfaces with more user-friendly laser systems will cause an even more rapid expansion of nonlinear spectroscopic studies. The need for more durable and efficient nonlinear crystals to generate infrared below 1800 cm^{-1}, where many important vibrational chromophores are resonant, would be most welcome. The study of time-dependent chemical and physical phenomena in ground and excited electronic and vibrational states will certainly increase as advances in commercial picosecond and femtosecond lasers are made. The development of new methods of preparation and handling of thin films, as well as new materials whose properties are controlled by interfaces, will provide a further driving force for nonlinear spectroscopic studies. As a parallel to these anticipated experimental advances, and most importantly in conjunction with them, is the strong need for increased theoretical and computer simulation contributions. Calculations of equilibrium and dynamic interface phenomena, ranging from interface structure, reactive potential surfaces, energetics, and phase transitions to calculations of molecular motions and excited state relaxation, are clearly essential to the further healthy development of this burgeoning field.

ACKNOWLEDGMENTS

The author thanks the National Science Foundation, Air Force Office of Scientific Research, and the Division of Chemical Sciences, US Department of Energy for their generous support.

Literature Cited

1. Adamson, A. W. 1982. *Physical Chemistry of Surfaces*. New York: Wiley. 4th ed.
2. Bloembergen, N. 1965. *Nonlinear Optics*. New York: Benjamin
3. Shen, Y. R. 1989. *Annu. Rev. Phys. Chem.* 40: 327–50
4. Richmond, G. L., Robinson, J. M., Shannon, V. L. 1988. *Prog. Surf. Sci.* 28: 1–70
4a. Heinz, T. F. 1991. *Nonlinear Surface Electromagnetic Phenomena*, ed. H. E. Ponath, G. I. Stegeman, pp. 353–416. Amsterdam: North-Holland
5. Williams, D. J., ed. 1985. *Nonlinear Optical Properties of Organic and Polymeric Materials. ACS Symp. Ser.* 233. Washington, DC: Am. Chem. Soc.
6. Heinz, T. F., Chen, C. K., Ricard, D., Shen, Y. R. 1982. *Phys. Rev. Lett.* 48: 478–81
7. Heinz, T. F., Tom, H. W. K., Shen, Y. R. 1983. *Phys. Rev. A* 28: 1883–85
8. Dick, B. 1985. *Chem. Phys.* 96: 199–215
9. Hicks, J. M., Kemnitz, K., Eisenthal, K. B. 1986. *J. Phys. Chem.* 90: 560–62
10. Mazely, T. L., Hetherington, W. M. III. 1987. *J. Chem. Phys.* 86: 3640–47
11. Berkovic, G. 1990. *Physica A* 168: 140–48
12. Hsiung, H., Meredith, G. R., Vanherzeede, H., Popovitz-Biro, R., Shavit, E., Lahav, M. 1989. *Chem. Phys. Lett.* 164: 539–44
13. Shirota, K., Kajikawa, K., Takezoe, H., Fukuda, A. 1990. *Jpn. J. Appl. Phys.* 29: 750–55
14. Vogel, V., Mullin, C. S., Shen, Y. R. 1991. *Langmuir* 7: 1222–24
15. Gennis, R. B. 1989. *Biomembranes*, pp. 235–56. New York: Springer-Verlag

16. Zhao, X., Goh, M. C., Eisenthal, K. B. 1990. *J. Phys. Chem.* 94: 2222–24
17. Higgins, D. A., Byerly, S. K., Abrams, M. B., Corn, R. M. 1991. *J. Phys. Chem.* 95: 6984–90
18. Peterson, E. S., Harris, C. B. 1989. *J. Chem. Phys.* 91: 2683–88
19. Kemnitz, K., Tamai, N., Yamazaki, I., Nakashima, N., Yoshihara, K. 1986. *J. Phys. Chem.* 90: 5094
20. Kemnitz, K., Bhattacharyya, K., Hicks, J. M., Pinto, G. R., Eisenthal, K. B., Heinz, T. F. 1986. *Chem. Phys. Lett.* 131: 285–90
21. Chang, R. K., Ducuing, J., Bloembergen, N. 1965. *Phys. Rev. Lett.* 15: 6
22. Wynne, J. J., Bloembergen, N. 1969. *Phys. Rev.* 188: 1211–20
23. Weyl, W. A. 1951. *J. Colloid Sci.* 6: 389
24. Stillinger, F. H., Ben-Naim, A. 1967. *J. Chem. Phys.* 47: 4431–47
25. Fletcher, N. H. 1968. *Philos. Mag.* 18: 1287
26. Townsend, R. M., Gryko, J., Rice, S. A. 1985. *J. Chem. Phys.* 82: 4391–92
27. Croxton, C. A. 1981. *Physica A* 106A: 239–59
28. Wilson, M. A., Pohorille, A., Pratt, L. R. 1987. *J. Phys. Chem.* 91: 4873
29. Matsumoto, M., Kataoka, Y. 1988. *J. Chem. Phys.* 88: 3233
30. Randles, J. E. B. 1977. *Phys. Chem. Liq.* 7: 107
31. Eley, D. D., Evans, M. G. 1938. *Trans. Faraday Soc.* 34: 1093
32. Saloman, M. 1970. *J. Phys. Chem.* 74: 2519
33. Gomer, R., Tryson, G. 1977. *J. Chem. Phys.* 66: 4413
34. Borazio, A., Farrell, J. R., McTigue, P. 1985. *J. Electroanal. Chem.* 193: 103
35. Zhou, Y., Stell, G., Friedman, H. L. 1988. *J. Chem. Phys.* 89: 3836
36. Goh, M. C., Hicks, J. M., Kemnitz, K., Pinto, G. R., Bhattacharyya, K., et al. 1988. *J. Phys. Chem.* 92: 5074–75
37. Levine, B. F., Bethea, C. G. 1976. *J. Chem. Phys.* 65: 2429
38. Goh, M. C., Eisenthal, K. B. 1989. *Chem. Phys. Lett.* 157: 101–4
39. Superfine, R., Huang, J. Y., Shen, Y. R. 1990. *Opt. Lett.* 15: 1276–78
40. Superfine, R., Huang, J. Y., Shen, Y. R. 1991. *Phys. Rev. Lett.* 66: 1066–69
41. Huang, J. Y., Lewis, A. 1989. *Biophys. J.* 55: 835–42
42. Sato, O., Baba, R., Hashimoto, K., Fujishima, K. 1991. *J. Phys. Chem.* 95: 9636–38
43. Hayden, L. M., Kowel, S. T., Srinivasan, M. P. 1987. *Opt. Commun.* 61: 351–56
44. Hsiung, H., Rodriguez-Parada, J., Bekerbaner, R. 1991. *Chem. Phys. Lett.* 82: 88–92
45. Hsiung, H. 1991. *Appl. Phys. Lett.* 59: 2495–97
46. Bain, C. D., Davies, P. B., Ong, T. H., Ward, R. N., Brown, M. A. 1991. *Langmuir* 7: 1563–66
47. Anderson, R. J. M., Hamilton, J. 1990. *High Temp. Sci.* 26: 1–17
48. Zhu, X. D., Daum, W., Xiao, X. D., Chin, R., Shen, Y. R. 1991. *Phys. Rev. B* 43: 11571–80
49. Bhattacharyya, K., Sitzmann, E. V., Eisenthal, K. B. 1987. *J. Chem. Phys.* 87: 1442–43
50. Castro, A., Bhattacharyya, K., Eisenthal, K. B. 1991. *J. Chem. Phys.* 95: 1310–15
51. Xiao, X. D., Vogel, V., Shen, Y. R. 1989. *Chem. Phys. Lett.* 163: 555–59
52. Hall, R. B., DeSantolo, A. M., Grubb, S. G. 1987. *J. Vac. Sci. Technol. A* 5: 865–66
53. Miragliotta, J., Polizzotti, R. S., Rabinowitz, P., Cameron, S. D., Hall, R. B. 1990. *Chem. Phys.* 143: 123–30
54. Meech, S. R., Yoshihara, K. 1990. *Chem. Phys. Lett.* 174: 423–27
55. Meech, S. R., Yoshihara, K. 1990. *J. Phys. Chem.* 94: 4913–20
56. Sitzmann, E. V., Eisenthal, K. B. 1988. *J. Phys. Chem.* 92: 4579–80
57. Sitzmann, E. V., Eisenthal, K. B. 1989. *J. Chem. Phys.* 90: 2831–32
58. Chuang, T. J., Eisenthal, K. B. 1971. *Chem. Phys. Lett.* 11: 368
59. Reiser, D., Laubereau, A. 1982. *Chem. Phys. Lett.* 92: 297
60. Rothschild, W. G. 1984. *Dynamics of Molecular Liquids*, pp. 67–185. New York: Wiley
61. Kinoshita, K., Kataoka, R., Gotoh, O., Ikegami, A. 1981. *Biochemistry* 20: 4270
62. Wolber, P. K., Hudson, B. S. 1981. *Biochemistry* 20: 2800
63. Szabo, A. 1984. *J. Chem. Phys.* 81: 150
64. Anfinrud, P. A., Hart, D. E., Struve, W. S. 1988. *J. Phys. Chem.* 92: 4067
65. Castro, A., Sitzmann, E. V., Zhang, D., Eisenthal, K. B. 1991. *J. Phys. Chem.* 95: 6752–53
66. Gomer, R. 1990. *Rep. Prog. Phys.* 53: 917
67. Hamers, R. J., Kohler, U. K., Demuth, J. E. 1989. *Ultramicroscopy* 31: 10
68. Reider, G. A., Hofer, U., Heinz, T. F. 1991. *Phys. Rev. Lett.* 66: 1994–97
69. Zhu, X. D., Raising, Th., Shen, Y. R. 1988. *Phys. Rev. Lett.* 61: 2883
70. Castro, A., Ong, S., Eisenthal, K. B. 1989. *Chem. Phys. Lett.* 163: 412–16
71. Raising, Th., Shen, Y. R., Kim, M. W.,

Grubb, S. 1985. *Phys. Rev. Lett.* 55: 2903–6
72. Zhao, X., Goh, M. C., Subrahmanyan, S., Eisenthal, K. B. 1990. *J. Phys. Chem.* 94: 3370–73
73. Zhao, X., Subrahmanyan, S., Eisenthal, K. B. 1991. *Phys. Rev. Lett.* 67: 2025
74. Reider, G. A., Hofer, U., Heinz, T. F. 1991. *J. Chem. Phys.* 94: 4080–83
75. Koehler, B. G., Mak, C. H., Arthur, A., Coon, P. A., George, S. M. 1988. *J. Chem. Phys.* 89: 1709
76. Sinniah, K., Sherman, M. G., Lewis, L. B., Weinberg, W. H., Yates, J. T. Jr., Janda, K. C. 1990. *J. Chem. Phys.* 92: 5700
77. Harris, A. L., Levinos, N. J. 1989. *J. Chem. Phys.* 90: 3878–79
78. Heilweil, E. J., Stephenson, J. C., Cavanagh, R. R. 1988. *J. Phys. Chem.* 92: 6099
79. Harris, A. L., Rothberg, L., Dubois, L. H., Levinos, N. J., Dhar, L. 1990. *Phys. Rev. Lett.* 64: 2086–89
80. Harris, A. L., Rothberg, L., Dhar, L., Levinos, N. J., Dubois, L. H. 1991. *J. Chem. Phys.* 94: 2438–47
81. Graener, H., Laubereau, A. 1987. *Chem. Phys. Lett.* 133: 378
82. Guyot-Sionnest, P., Dumas, P., Chabal, Y. J., Higashi, G. S. 1990. *Phys. Rev. Lett.* 64: 2156–59
83. Chabal, Y. J., Dumas, P., Guyot-Sionnest, P., Higashi, G. S. 1991. *Surf Sci.* 242: 524 30
84. Harris, A. L., Rothberg, L. 1991. *J. Chem. Phys.* 94: 2449–57
85. Heinz, T. F., Palfrey, S. L., Eisenthal, K. B. 1984. *Opt. Lett.* 9: 359–61
86. Superfine, R., Huang, J. Y., Shen, Y. R. 1990. *Chem. Phys. Lett.* 172: 303–6
87. Wiberg, K. B., Wendoloski, J. J. 1984. *J. Phys. Chem.* 88: 586
88. Galabov, B., Dirdev, T., Durig, J. R., Orville-Thomas, W. J. 1988. *J. Mol. Struct.* 173: 111
89. Haskett, D., Song, K. J., Burns, A., Plummer, E. W., Dai, H. L. 1986. *J. Chem. Phys.* 85: 7490–92
90. Demuth, J. E., Christmann, K., Sanda, P. N. 1980. *Chem. Phys. Lett.* 76: 201–6
91. Lee, C. H., Chang, R. K., Bloembergen, N. 1967. *Phys. Rev. Lett.* 18: 167
92. Guyot-Sionnest, P., Tadjeddine, A., Liebsch, A. 1990. *Phys. Rev. Lett.* 64: 1678–81
93. Georgiadis, R., Neff, G. A., Richmond, G. L. 1990. *J. Chem. Phys.* 92: 4623–25
94. Bradley, R. A., Arekat, S., Georgiadis, R., Robinson, J. M., Kevan, S. D., Richmond, G. L. 1990. *Chem. Phys. Lett.* 168: 486–72
95. Guyot-Sionnest, P., Tadjeddine, A. 1990. *Vacuum* 41: 720–22
96. Guyot-Sionnest, P., Tadjeddine, A. 1990. *J. Chem. Phys.* 92: 734–38
97. Rojhantalab, H. M., Richmond, G. L. 1989. *J. Phys. Chem.* 93: 3269
98. Tadjeddine, A., Guyot-Sionnest, P. 1990. *J. Phys. Chem.* 94: 5194–95
99. Lupke, G., Marowsky, G., Steinhoff, R., Friedrich, A., Pettinger, B., Kolb, D. M. 1990. *Phys. Rev. B* 41: 6913–19
100. Lynch, M. L., Corn, R. M. 1990. *J. Phys. Chem.* 94: 4382–85
101. Koos, D. A., Shannon, V. L., Richmond, G. L. 1990. *J. Phys. Chem.* 94: 2091–98
102. Koos, D. A., Richmond, G. L. 1990. *J. Chem. Phys.* 93: 869–71
103. Robinson, J. M., Richmond, G. L. 1990. *Chem. Phys.* 141: 175–88
104. Campbell, D. J., Higgins, D. A., Corn, R. M. 1990. *J. Phys. Chem.* 94: 3681–89
105. Guyot-Sionnest, P., Tadjeddine, A. 1990. *Chem. Phys. Lett.* 172: 341–45
106. Ashley, K., Samant, M. G., Seki, H., Philpott, M. R. 1989. *J. Electroanal. Chem.* 270: 349–64

Annual Review of Physical Chemistry
Volume 43, 1992

CONTENTS

(*continued*) vii